Carbon 158 (2020) 137–145

Contents lists available at ScienceDirect

Carbon

journal homepage: www.elsevier.com/locate/carbon

An ultralight, supercompressible, superhydrophobic and multifunctional carbon aerogel with a specially designed structure

Sishi Long [a], Yunchao Feng [a], Faliang He [d], Shuaishuai He [a], Huachi Hong [a], Xuerui Yang [a], Lingling Zheng [e], Jian Liu [a, b, c, *], Lihui Gan [a, b, c, **], Minnan Long [a]

[a] College of Energy, Xiamen University, Xiamen, 361102, China
[b] Fujian Engineering and Research Center of Clean and High-valued Technologies for Biomass, Xiamen University, Xiamen, 361102, China
[c] Xiamen Key Laboratory of High-valued Conversion Technology of Agricultural Biomass, Xiamen University, Xiamen, 361102, China
[d] Department of Physics, Research Institute for Biomimetics and Soft Matter, Xiamen University, Xiamen, 361005, China
[e] Pen-Tung Sah Institute of Micro-Nano Science and Technology Xiamen University, Xiamen, 361005, PR China

ARTICLE INFO

Article history:
Received 29 August 2019
Received in revised form
17 November 2019
Accepted 22 November 2019
Available online 27 November 2019

Keywords:
Carbon aerogel
Nanofibrillated cellulose
Kaolin
Graphene oxide
Oil/water separation
Pressure sensors

ABSTRACT

Compressible and ultralight carbon aerogels are attractive due to its compressibility, elasticity and conductivity. However, it is still a great challenge to enrich the properties of carbon aerogel to meet various requirements. Herein, we report an untralight, supercompressible, fatigue resistant, superhydrophobic and fire-resistant and multifunctional CNF-GO/glucose-kaolin carbon aerogel (C-NGGK) carbon aerogel. To achieve such excellent performances, calcined GO, CNFs, glucose and kaolin are used for forming low-density and continuous wave-shape rGO layers, reinforcing the mechanical strength of carbon layers, realizing superelasticity and fatigue resistance and resulting in a superhydrophobic surface for C-NGGK, respectively. The as-prepared C-NGGK demonstrates excellent superhydrophobicity with the water contact angle (WCA) of 124.9°, and the absorption efficiency of the C-NGGK samples for different oils and organic solvents are 75–255 times their own weight. These advantages show that the C-NGGK can be an ideal candidate for oil/water separation. In addition, there is also the prospect to be used for pressure sensors, while other potential applications include three-dimensional electrode materials for supercapacitors and batteries, catalyst carriers and various wearable devices.

1. Introduction

Carbon aerogels with interconnected three-dimensional (3D) networks have raised extensive attention due to their fascinating features, such as low density, chemical stability, large surface area, high electrical conductivity, rich porosity and lightweight [1–4]. Therefore, carbon aerogels are potential alternatives applied as absorbents [5–8], catalyst supports [9,10], electrodes for supercapacitors [11–13], lithium-ion batteries [14,15] and sensors [16,17]. Especially, compressibility or ultralight carbon aerogels are more attractive for its potential multifunctional property. For example, ultra-flyweight all carbon aerogel can be used as an ideal candidate for the absorbent of organics or the active electrode material [18]; flexible and fire-resistant carbon nanofiber aerogels, fabricated by carbonized bacterial cellulose, exhibits high stability of electronic conductivity, as well as excellent adsorption as absorbents [19].

Carbon aerogels are conventionally prepared using resorcinol-formaldehyde as precursors via a sol-gel and high temperature carbonization (inert atmosphere) process [20], however, the prepared carbon aerogels are fragile and show a high density [21,22]. New emerged carbon aerogels such as three-dimensional porous graphene sponges [23], carbon nanotube sponges [8], grapheme or grapheme oxide (GO) and carbon nanotube-based foam [7], and chemically modified graphene carbon aerogels [24] have attracted great attention because they can be used as building units and translated into 3D monolithic carbon material [25,26]. Among them, GO is a one of the most promising building block for 3D architectures due to its 2D morphology and excellent dispersion in water. Several reports concerned the use of solvothermal [27], freeze-drying [18,28–30] and chemical vapor deposition (CVD) [31,32] for the synthesis of compressible 3D carbon aerogels.

* Corresponding author. College of Energy, Xiamen University, Xiamen, 361102, China.
** Corresponding author. College of Energy, Xiamen University, Xiamen, 361102, China.
E-mail addresses: jianliu@xmu.edu.cn (J. Liu), ganlihui@xmu.edu.cn (L. Gan).

https://doi.org/10.1016/j.carbon.2019.11.065
0008-6223/

However, the further potential of these technologies is hindered by poor mechanical performance (solvothermal, freeze-drying) and high-cost (CVD). Alternatively, directional freezing is a simple and novel method for preparing 3D monolithic structures [30]. For example, superelastic 3D graphene-based cellular monoliths with high strength were fabricated by directional freezing [28]. However, the plastic deformation ability decreased on the cyclic compression at a high compressive strain because of the restack of graphene sheets. To improve the mechanical robustness of GO-based aerogels, carbon nanotubes (CNTs) [18], chitosan [33], cellulose nanocrystals (CNCs) [29] and other polymer foams [34,35] have been used to prevent the restack of graphene sheets. Despite the great advancement, the application of these fabricated advanced 3D monoliths largely depends on their compressibility, elasticity and conductivity. Therefore, it is still a great challenge to enrich the properties of carbon aerogel to meet various requirements.

Cellulose nanofiber (CNF) as an abundant and renewable biomass material shows great potential as support, building block and cross-linker due to its interconnected networks of 1D nanofibers and robust mechanical property [36–38]. Consequently, water-insoluble dopants such as Kaolin clay (a common and cheap mineral) can be well dispersed in CNF solution. Herein, we report a CNF-GO/glucose-kaolin carbon aerogel (C-NGGK) with superior mechanical properties, superhydrophobicity and high sensitivity. In order to achieve such excellent performances, calcined GO, CNFs, glucose and kaolin are used for forming low-density and continuous wave-shape rGO layers, reinforcing the mechanical strength of carbon layers, realizing superelasticity and fatigue resistance and resulting in a superhydrophobic surface for C-NGGK, respectively. The as-fabricated C-NGGK carbon aerogel shows untralight, supercompressible, fatigue resistant, superhydrophobic and fire-resistant. When used as absorbents, the C-NGGK exhibits an outstanding reversible adsorption capacity for a wide range of oils and organic solvents. In addition, the electrical conductivity of the C-NGGK is highly responsive to compressive strain, which makes it a potential material for pressure sensing.

2. Experimental section

2.1. Materials

Graphene oxide (GO) was purchased by Suzhou TANFENG Science Tech Co. Ltd. (Suzhou, China). Eucalyptus pulp was supplied from Asia Symbol Pulp and Paper Co. Ltd. (Shandong, China). Hydrochloric acid (HCl), sodium hypochlorite (NaClO), sodium hydroxide (NaOH), glucose and kaolin were supplied by Aladdin Chemical Technology Co. Ltd. (Shanghai, China). Deionized water (DIW) was used throughout the experiment. All chemicals are of reagent grade without any further purification.

2.2. Preparation of CNF

The CNF suspension of 1.0 wt% was prepared by TEMPO method according to the previous literature [39]. The eucalyptus pulp (3.33 g, containing 1 g of cellulose fibers) was suspended in DIW (100 mL) containing sodium bromide (0.1 g) and TEMPO (0.016 g). 12% NaClO solution was adjusted to pH 10 with 0.1 M HCl, and then added into the eucalyptus pulp suspension at room temperature. The pH was adjusted to 10 by adding 0.5 M NaOH. The TEMPO-oxidized cellulose was then thoroughly washed and suspended with DIW to form slurry. Finally, the CNF dispersion was obtained by using a kitchen blender to agitate the TEMPO-oxidized cellulose for 15 min.

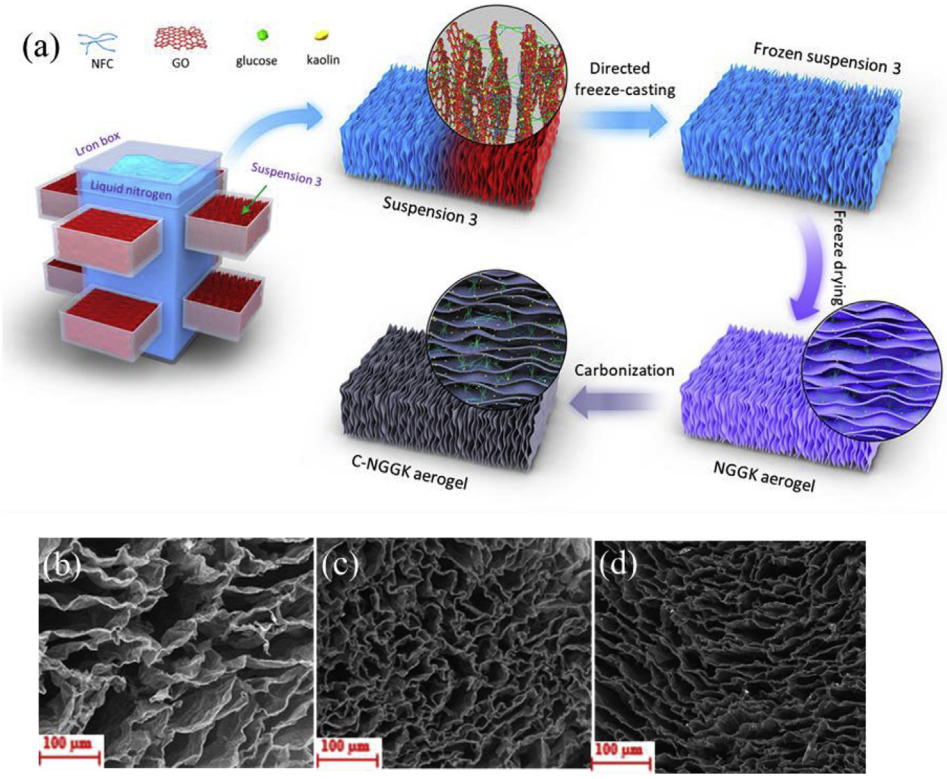

Fig. 1. Fabrication, microstructures and mechanical property of C-NGGK. a)The preparation of C-NGGK via a directional freezing method. b-d) SEM images of C-aerogel 2, C-aerogel 5 and C-NGGK, respectively. The scale bars represent 100 μm. (A colour version of this figure can be viewed online.)

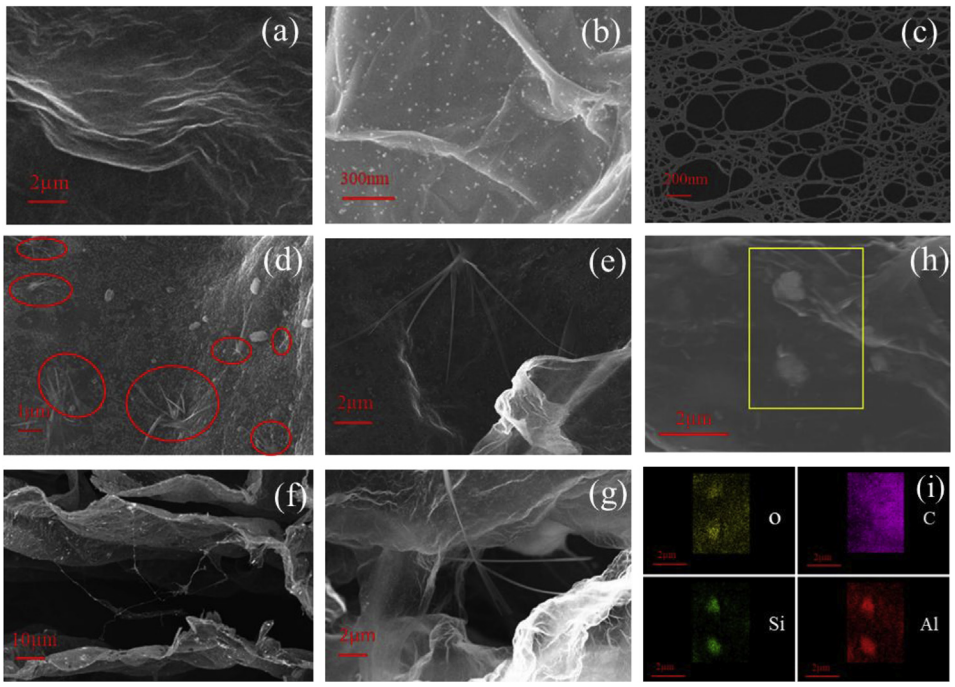

Fig. 2. a) SEM image of rGO sheet of C- aerogel 1, no carbon dot is detected. b) SEM image of carbonized glucose on rGO sheet. c) SEM images of the CNF aerogel with interconnected long nanofibers networks. d,e) Carbonized CNFs are like grass growing on the surface of wave-shape layers in clusters. f,g) Carbonized CNFs are like tapes connecting the wave-shape layers. h) The carbonized kaolin is uniformly distributed on the rGO sheet. i) EDS mapping images of C-NGGK. (A colour version of this figure can be viewed online.)

2.3. Fabrication of CNF-GO/glucose-kaolin suspension

Firstly, GO (150 mg) was dispersed in DIW (110 mL), stirred for 15 h and ultrasonicated for 3 h to get Suspension 1. CNF suspension (1.0 wt%, 40 g, containing 400 mg CNF) was then added, stirred for 2 h and ultrasonicated for 1 h to get Suspension 2. Afterwards, glucose (200 mg) and kaolin (300 mg) were added to prepare the CNF-GO/glucose-kaolin suspension (Suspension 3). For comparison, Suspension 4 (GO-glucose, without addition of CNF and kaolin) and Suspension 5 (CNF-GO/glucose, without addition of kaolin) were also prepared with the same process.

2.4. Fabrication of C-NGGK

The prepared suspension was injected into a plastic container and tied to a non-covered steel tank filled with liquid nitrogen for the freeze casting. Then, the samples were freeze-dried to obtain aerogels, named as Aerogel 1 (from Suspension 1), Aerogel 2 (from Suspension 2), NGGK (from Suspension 3), Aerogel 4 (from Suspension 4) and Aerogel 5 (from Suspension 5). The aerogels were subjected to pyrolysis in a tube furnace from about 20 °C to 700 °C at a heating rate of 3 °C/min under the atmosphere of nitrogen, and kept at 700 °C for 2 h to prepare carbon aerogels, named as C-aerogel 1, C-aerogel 2, C-NGGK, C-aerogel 4 and C-aerogel 5, respectively.

2.5. Absorption of organic solvents and oils by the C-NGGK

The absorption capacity of the C-NGGK samples for 20 kinds of organic solvents and oils was measured. The C-NGGK samples were immersed into the organic liquids for approximately 30 s and then taken out for further investigation.

The weight of C-NGGK samples before and after absorption was checked for calculating the absorption capacity (Q) as follows (1):

$$Q = (M_t - M_0)/M_0 \quad (1)$$

Where, M_0 and M_t are the weight of the aerogel before and after absorption, respectively. Each organic solvent or oil was tested for three times and the mean Q was recorded. To study the reusability of the as-prepared C-NGGK samples, the absorbed organic solvents or oils can be directly burned in air or distilled to recycle the used carbon aerogel. The regenerative aerogel retested for the absorption again.

2.6. Characterizations

Micromorphology was observed on TEM (Tecnai Spirit (T12), Netherlands) and SEM (SUPRA 55 instrument (Zeiss Sigma)). The samples were characterized by an Ultimate IV (Rigaku, Japan) X-ray diffraction (XRD) spectrometer and a DXR (American Thermo Electron) Raman spectrometer operating with 532 nm laser. Compression, elasticity and cycling tests were carried out by an Instron (microtester 5948) with a 100 N load cell. The samples (C-NGGK, 20 mm × 18 mm × 11 mm) were loaded between two compression stages, and compressed or released vertically with the top stage. For wavy layered structure, the direction of compression is perpendicular to the layered structure. The speed of all sample compression tests is 0.5 mm s^{-1}. The resistance of carbon aerogel was determined using a multimeter (VC 890D). The electrical current was measured with an electrochemical workstation (CHI660E).

2.7. Assembly and testing of C-NGGK sensor

The C-NGGK sensor was assembled by incorporating C-NGGK into two copper tapes (electric contacts) adhered to thick poly(-ethylene terephthalate) (PET) substrates. In order to facilitate electrical contact, silver paste is brushed to both ends of the carbon aerogel before loading the copper tapes. The real-time resistance

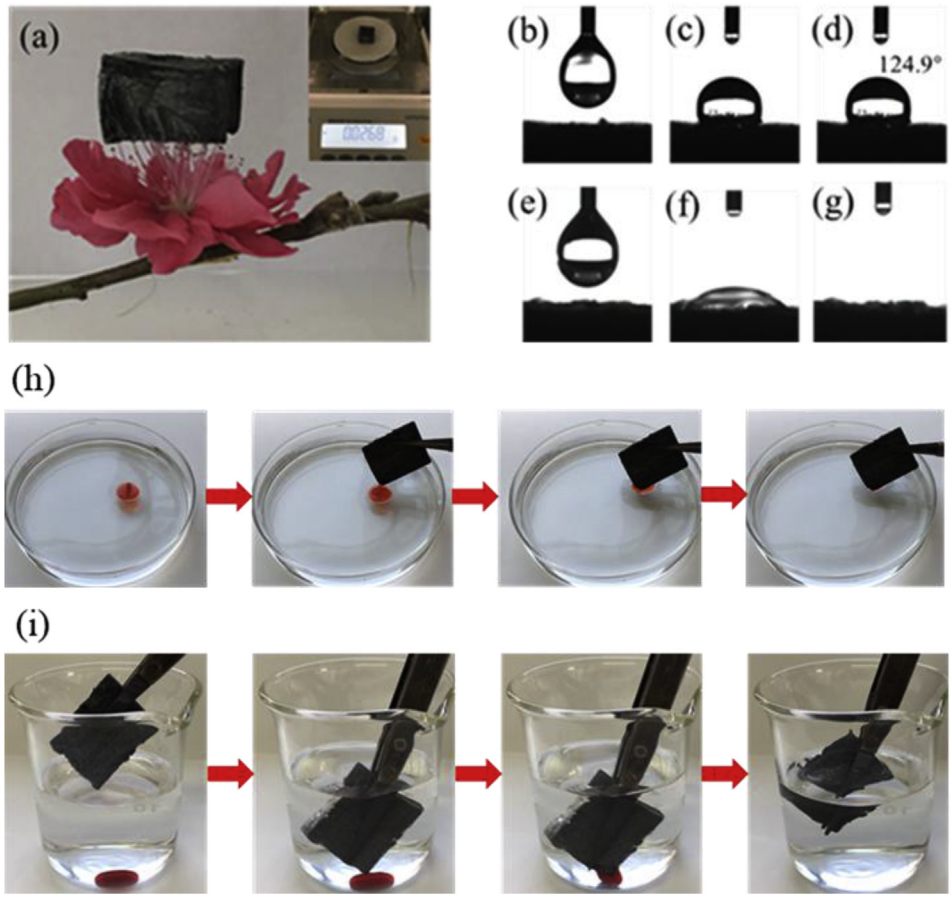

Fig. 3. a) The ultralight C-NGGK, supported by stamens. Video snapshots for the wetting behavior of a water droplet (b, c, d) and a soybean oil droplet (e, f, g) placed onto the surface of C-NGGK. Absorption of pump oil from the surface of water (h) and CCl_4 from underwater (i) by C-NGGK. The CCl_4 and pump oil were colored with Sudan III for clear presentation. (A colour version of this figure can be viewed online.)

signals were recorded on a TH2829A precision LCR meter and output by Labview.

3. Results and discussion

As shown in Fig. 1a, the supercompressible, superelastic and superhydrophobic carbon aerogel (C-NGGK) is fabricated by mixing glucose, CNF and kaolin in GO aqueous solution, directional freeze-casting, freeze-drying and carbonization. CNF is chosen to act as nano reinforcement to improve the mechanical property of GO based aerogel. Besides, CNF can disperse GO and kaolin in aqueous solution. CNF and glucose are used as carbon precursors to ensure superelasticity and fatigue resistance of rGO layers on being compressed by external force. Since carbonized kaolin has excellent hydrophobicity, the addition of kaolin as a precursor of C-NGGK contributes to the formation of hydrophobic composite carbon aerogel. On directional freezing, the water formed into ice crystals to squeeze GO sheets and CNF, thereby forming wave-shape layers structure, even retained after carbonization (Fig. 1b–d). C-aerogel 2 (Fig. 1b), C-aerogel 5 (Fig. 1c), and C-NGGK (C-aerogel 3, Fig. 1d) have continuous wave-shape rGO layers.

As shown in Figs. S1a, b, d (support information), Aerogel 1 and Aerogel 4 underwent significant deformation in freeze-drying when compared with Aerogel 2. After carbonization, C-aerogel 1 and C-aerogel 4 further shrunk or deformed significantly (Figs. S1a and d), while most of the volume of C-aerogel 2 retained (Fig. S1b). However, NGGK and Aerogel 5 (Figs. S1c and e) can maintain their shape sizes perfectly after freeze-drying or carbonization. It seems that CNFs can be used as reinforcements for nanocomposites to prevent GO-base aerogel from shrinking or deforming during freeze-drying and carbonization. The lower volume shrinkage indicates that CNFs act as the key nano-structural material to support the ultralight carbon aerogel (Figures S1b, c and e).

GO is converted into rGO in the annealing, and on the rGO sheet, no carbon dot is detected (Fig. 2a), and glucose is transformed into carbon dots that dispersed and adhered onto the rGO sheets (Fig. 2b). Carbon dots may have the potential to strengthen the interaction between the layers of hierarchical wave-shape architecture. CNFs, derived from renewable cellulose, have exhibited excellent mechanical properties [40,41] and high aspect ratio, and would be an ideal precursor for forming interconnected 3D networks. SEM result shows a network structure of CNFs in which long nanofibers cross-linked each other (Fig. 2c). The carbonized CNF in C-NGGK shows two kinds of appearance. One is like grass, growing on the surface of wave-shape layers in clusters (Fig. 2d,e and Figs. S2a–d).The other is like tapes connecting wave-shape layers (Fig. 2f and g Figs. S2e–h). The existence of grass-like and tape-like carbonized CNF are beneficial to the enhancement of resistance to deformation and acts as a nano-enhancement or support. The carbonized kaolin is uniformly distributed on the rGO sheet (Fig. 2h). The elemental mappings (Fig. 2i) reveal the distribution of C, O, Si and Al elements on the rGO sheet, indicating the existence of kaolin in the C-NGGK.

Figure S3a demonstrates the D band at ~1345 cm^{-1} and the G

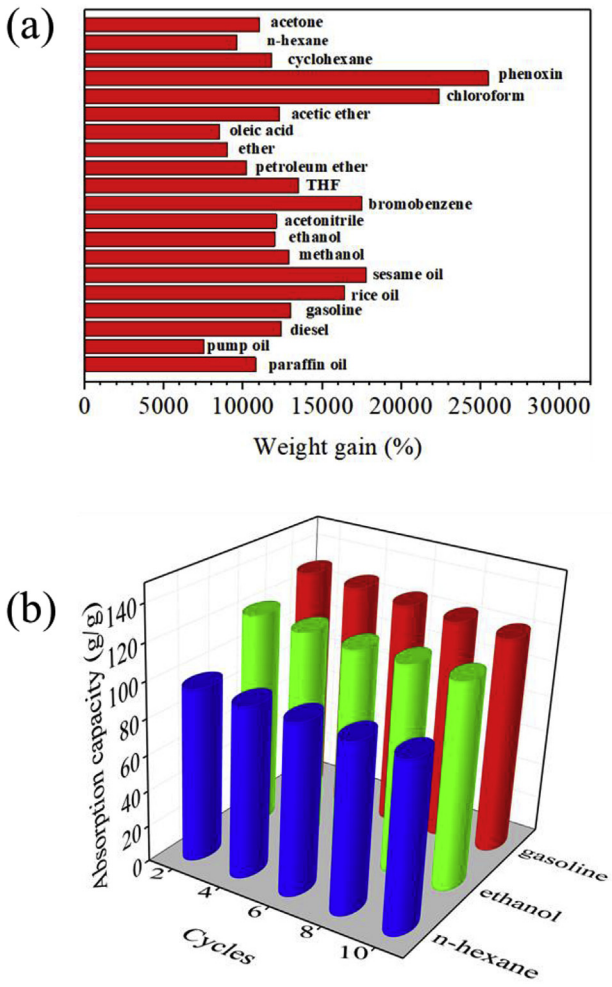

Fig. 4. a) Absorption capacity of C-NGGK samples for various organic liquids. b) Recyclability of C-NGGK samples for absorption of organic liquids. (A colour version of this figure can be viewed online.)

band at ~1580 cm^{-1} in the Raman spectra of C-NGGK, C-aerogel 2 and C-aerogel 5. The D band reflects the disorders or defects of carbon, whereas the G band is a characteristic feature of ordered carbon [42,43]. The intensity ratios of the G bands to D bands range from 1.05 to 1.08, showing no obvious difference, indicating that CNF and glucose were transformed into low-degree graphitized carbon in the carbonization process. The X-ray diffraction (XRD) patterns are shown in Fig. S3b. The prepared samples (C-NGGK, C-aerogel 2 and C-aerogel 5) exhibited the same broad low-intensity peak at $2\theta = 25.5°$, belonging to the (002) reflection of graphite, which confirmed a low-degree graphitization.

Interestingly, The as-synthesized C-NGGK(4 cm^{-3})can stand stably on top of stamens (Fig. 3a), attributed to its ultra-low density (6.7 mg cm^{-3}). Fig. 3b–d and Fig. S4 show the wetting behavior of a water droplet on the surface of the C-NGGK, C-aerogel 2 and C-aerogel 5, indicating the crucial role of kaolin for hydrophobicity. The C-NGGK exhibited surface hydrophobicity with a water contact angle of 124.9°, and a water droplet was sucked into C-aerogel 2 or C-aerogel 5 quickly. When C-NGGK is immersed into water by an external force, the entrained air bubbles at the interface between C-NGGK and the surrounding water can be observed clearly (Fig. S5), and a mirror effect is created. The reason for this phenomenon is attributed to the addition of kaolin. Kaolin as an abundant and budget mineral is a potential candidate to modify the composite carbon aerogel. The hydrophobic role of kaolin was checked by FT-IR spectroscopy as shown in Fig. S6, the hydrophilic groups (-OH) of calcinated kaolin disappeared. Accordingly, absorption bands intensity of kaolin doped carbon aerogel (C-NGGK) became extremely weak at 3455 cm^{-1} (stretching vibration O–H), leading to the formation of hydrophobic groups and contributing to oil/water separation. The C-NGGK exhibits higher absorption capacity than other typical carbonaceous absorbents (Table S1). Fig. S7a shows the long-time float on the water surface of C-NGGK due to the hydrophobic nature. In contrast, a soybean oil droplet was quickly sucked into the C-NGGK (Fig. 3e–g; Fig. S7b). Clearly, the carbon aerogel has satisfying oleophilic property (as evidenced by contact angle of 0°). As shown in Movie S1 and Fig. 3h, when the carbon aerogel was forced to contact with a drop of pump oil floating on the surface of water, the pump oil was completely absorbed in a few seconds. Moreover, the C-NGGK can be used to collect CCl_4 from underwater (Fig. 3i; Movie S2). Therefore, the C-NGGK is an ideal adsorbent for the selective removal of oils and organic solvents from water.

Supplementary video related to this article can be found at https://doi.org/10.1016/j.carbon.2019.11.065.

As shown in Fig. 4a, the absorption efficiency of the carbon aerogel for organic solvents and oils are 75–255 times its own weight, depending on the viscosity, density and surface tension of the organic solvents and oils, which are common pollutants in industry or daily life. Recycling the C-NGGK and recovering adsorbed liquid can greatly reduce the cost of oil-spill treatment. As shown in Fig. 4b, due to the high porosity and low density, these organic molecules can be absorbed and kept in the pores of the as-prepared C-NGGK. The absorption efficiency of the sample exhibits slightly decline with the absorption cycles increasing, and the tendencies of absorption efficiency to the 20 kinds of solvents are different, which may be related to the difference in the inherent stability of structure towards each solvent. Fig. S8 shows the recyclability of the C-NGGK absorbed gasoline, and it is regenerated by directly burning in air. The C-NGGK shows excellent fire resistance. Furthermore, C-NGGK retains a three-dimensional network after absorption and combustion, so it can be recycled for multiple times. Moreover, distillation was adopted as an alternative process for regeneration. After absorption, the absorbed n-hexane in C-NGGK was released by heating to its boiling point (69 °C), and then the vapor was collected for recycling, while the C-NGGK was regenerated (Fig. S9). The results clearly show C-NGGK has a high reversible ability to adsorb oils and organic solvents and can be recycled for multiple times.

Carbon aerogels generally have the disadvantages of lack resilience and fatigue resistance, and are prone to irreversible deformation under external mechanical forces. However, the as-prepared C-NGGK exhibits excellent elasticity and flexibility (Movie S3). As shown in Fig. 5a and Fig. S10a, the C-NGGK be compressed by more than 90%, and can return its original shapes without structural failure. However, C-aerogel 1 permanently collapsed and cannot recover to its original appearance after releasing the loading in Fig. 5b and Fig. S10b. As shown in Fig. 5c and d and Table S2, C-aerogel 2 can undergo 1000 cycles of compression-resilience at a strain of 50%, retaining 86.5% of its initial height and 76.4% of stress. The compression and resilience properties of C-aerogel 5 are remarkably improved by adding glucose (Fig. 5c, e). The C-aerogel 5 can almost maintain the initial height and 77.2% of stress after 2000 cycles under a strain of 50% (Fig. 5c, e and Table S2). As shown in Fig. 5c, f and Table S2, when kaolin was further added, it was found that the stiffness and strength of the carbon aerogel (C-NGGK) was enhanced and excellent fatigue resistance was kept. The C-NGGK can maintain a high stress (88.1%) and almost completely recover to the original height after 2000 cycles under a strain of 50%. It can be seen from

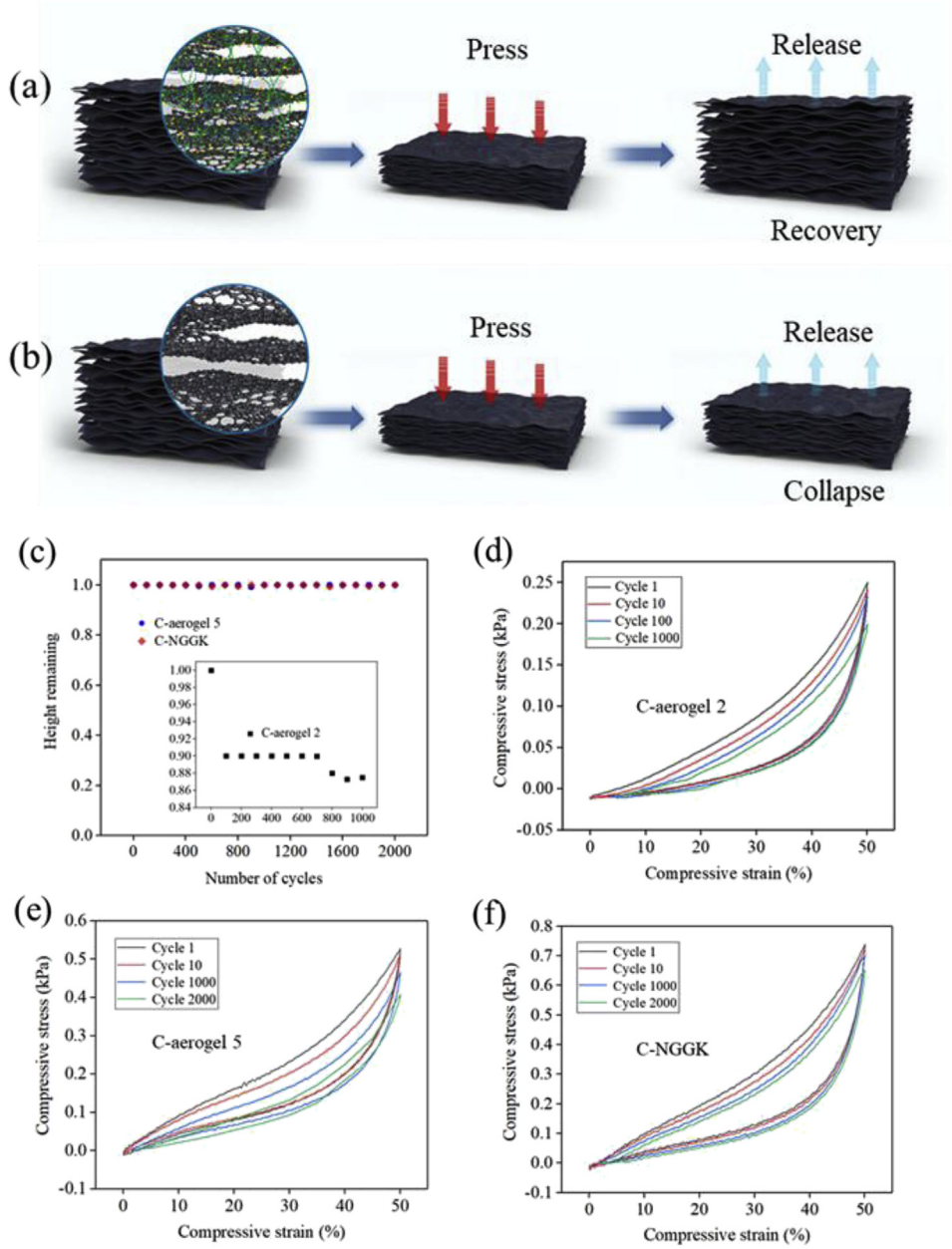

Fig. 5. a) The super compression and elasticity mechanisms of C-NGGK. b) The compression and collapse of C-aerogel 1 during compressing. c) Height retentions of carbon aerogels after repeated compression at a strain of 50%. d) Stress–strain curves of C-aerogel 2 for up to 1000 cycles. e) Stress–strain curves of C-aerogel 5 for up to 2000 cycles. f) Stress–strain curves of C-NGGK for up to 2000 cycles. (A colour version of this figure can be viewed online.)

Fig. 5d, e and f that the mechanical resilience of the carbon aerogels during compression is considered to be a typical viscoelastic behavior (all samples have hysteresis loops), and this phenomenon occurs in almost all compressible carbonaceous materials [31,44–47].

Supplementary video related to this article can be found at https://doi.org/10.1016/j.carbon.2019.11.065.

Fig. 6a shows the compressive stress-strain of the C-NGGK when the maximum value of ε is 30%, 60% and 90%, respectively. In the stress loading test, a linear-elastic region (ε< 65%) and a non-linear region (ε> 65%) were observed. The compressive stress increased gradually with the strain in the linear region, due to the elastic properties of the carbon aerogel. On the other hand, since the wave-shape layers of carbon aerogel interact upon each other and create a densification region, the stress rises sharply with compression in the non-linear region. As shown in Fig. 6b and Fig. S11, the as-prepared C-NGGK displays supercompressibility and elasticity. It can bear a strain of 90%, and nearly 100% of its initial height and wave-shape layers structure are retained after 100 cycles, showing excellent fatigue resistance and structural robustness. As shown in Fig. 6c, the strength or stiffness of C-NGGK was not significantly decreased by the compression of 100 cycles at a strain of 90%, retaining 79% of the original Young's modulus and maximum stress. The C-NGGK showed hysteresis loops by100 cyclic compressions at a strain of 90%. For the first cycle, the energy loss coefficient is 0.49. After 10 cycles, a nearly constant energy loss coefficient of 0.4 was obtained. Fig. 6d shows the energy loss coefficient of C-NGGK with compression strains up to 90%, which is much lower than

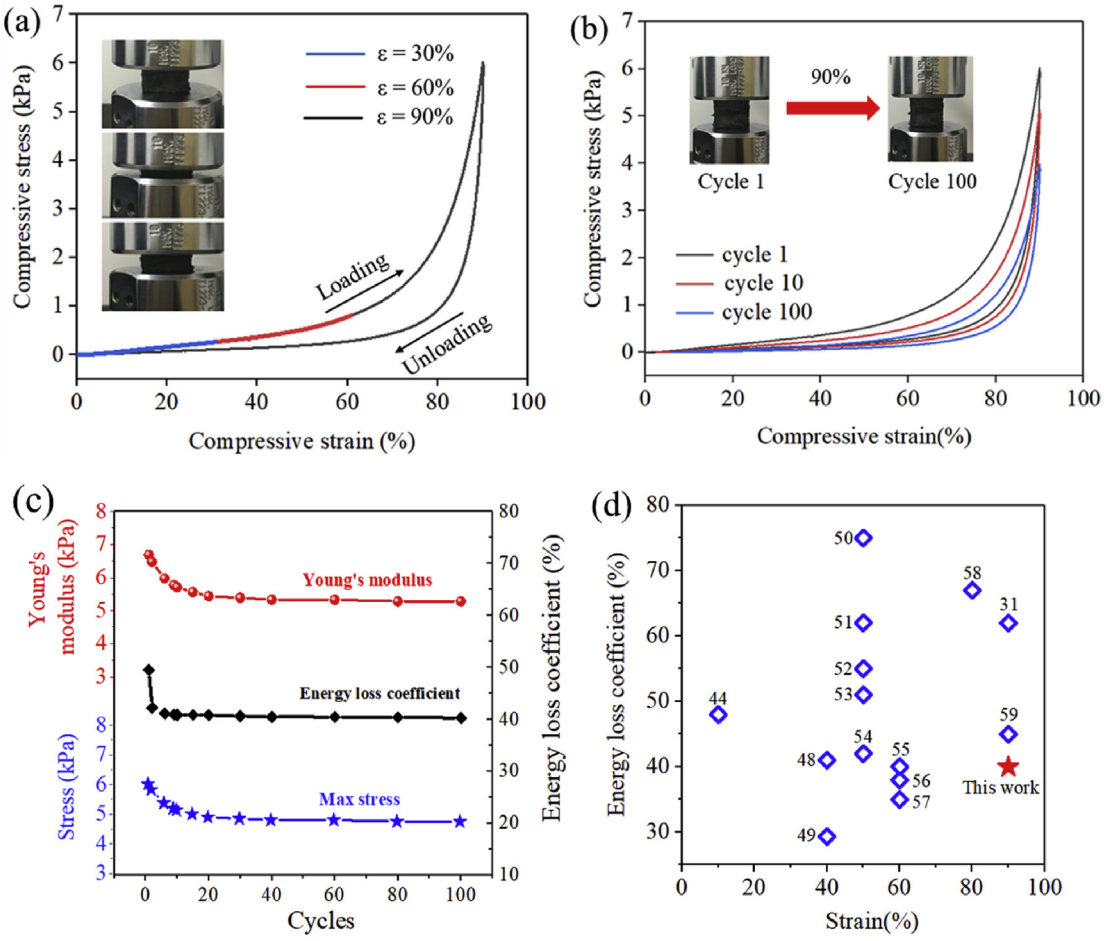

Fig. 6. Supercompressibility, superelasticity, fatigue resistance and pressure response of C-NGGK. a) Compressive stress–strain curves of C-NGGK at different set ϵ maximum value of 30, 60 and 90%. The photos of the C-NGGK in the compression process are shown in the insets. b) Stress-strain curves of C-NGGK for 100 cycles at a strain of 90%. c) The maximum stress, Young's modulus and energy loss coefficient of C-NGGK for the first 100 compression cycles at 90% strain. d) energy loss coefficient of C-NGGK and other previously reported materials. Numbers in the charts represent relevant references. (A colour version of this figure can be viewed online.)

previously reported work [31,44,48–59]. Consequently, C-NGGK exhibits excellent compressive recoverability, high strength and low energy dissipation.

The as-synthesized C-NGGK exhibits a high conductivity of 16.13 S m^{-1}, which gives it potential applications in electronic devices. The compressible and conductive properties of C-NGGK determine its pressure response. As shown in Fig. 7a, when the compressive strain is less than 65%, the electrical resistance shows nearly linear negative correlation, indicating the contact area increases rapidly with the compressive strain owing to the multi-

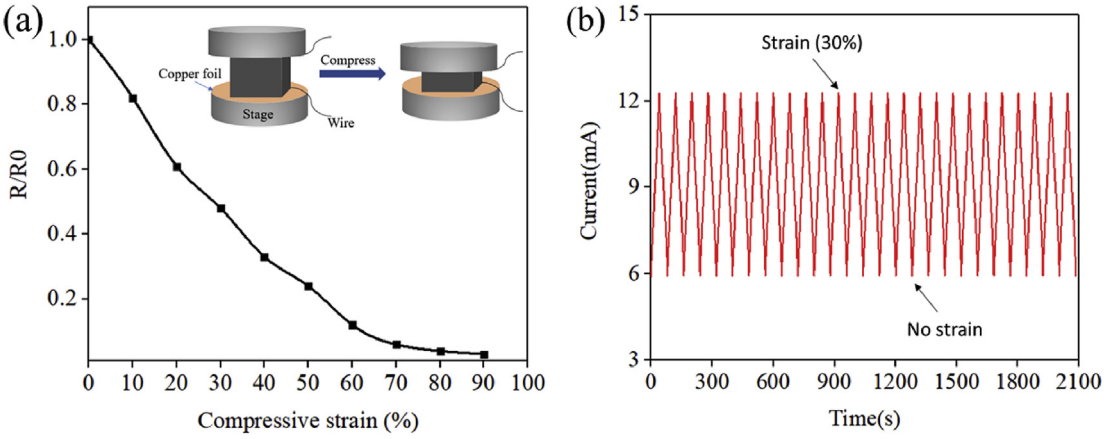

Fig. 7. a) The variation of electric resistance respect to compressive strain. The determination of the electric resistance in the compression process is shown in the insets. b) The electric current variation with cyclic compression strain of 0–30% in a closed circuit. (A colour version of this figure can be viewed online.)

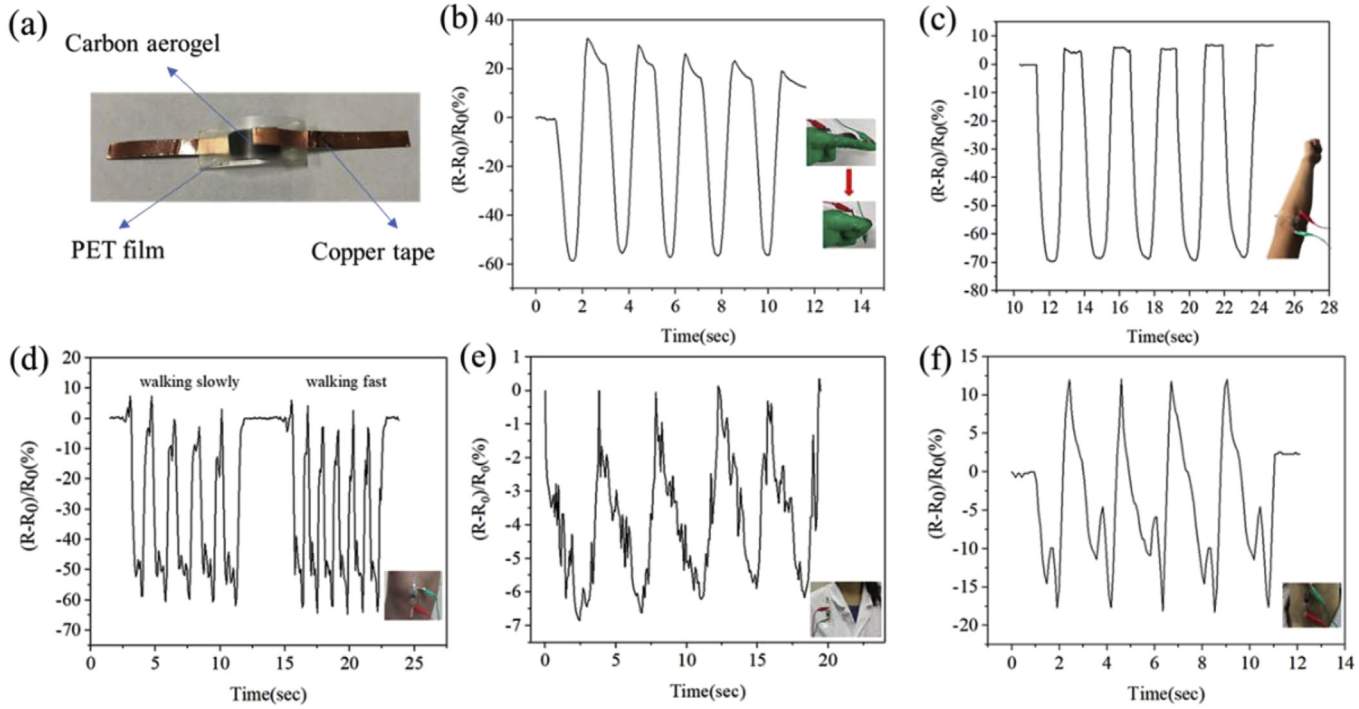

Fig. 8. Applications of the C-NGGK pressure sensor for the detection of human motion. a) The assembly of C-NGGK pressure sensor. b) The relative variations of resistance in the sensor from finger bending. (c) The relative variations of resistance in the sensor from elbow bending. d) The relative variations of resistance in the sensor attached on the knee joint caused by walking. e) The relative variations of resistance in the sensor caused by respiration. f) The relative variations of resistance in the sensor caused by swallowing. (A colour version of this figure can be viewed online.)

porous structure among wave-shape layers. The electrical resistance decreases slowly on the further increase of compressive strain, because the wave-shape layers have been densified, and it is difficult to form new interface contact spots. Besides, as shown in Movie S4 and Fig. S12, when C-NGGK acts as an elastic conductor, a diode light can be illuminated, and when it is compressed and released, the brightness of diode light fluctuates obviously. As shown in Fig. 7b, under a cyclic compression strain between 0 and 30%, the wavelength and amplitude of electric current is almost constant in the repetitive test. The results again show that the C-NGGK is of superelasticity and excellent fatigue resistance, resulting in an ultra-stable structure. Therefore, the continuous change of current with the high reversibility and compressive strain will give this kind of newly developed carbon aerogel the potential to be an excellent sensor with highly sensitivity.

Supplementary video related to this article can be found at https://doi.org/10.1016/j.carbon.2019.11.065.

The practical applications of the C-NGGK pressure sensor for human activity monitoring is investigated. Fig. 8a shows the assembly of C-NGGK into a simple pressure sensor device. The C-NGGK pressure sensor is used to detect both large body motions (including walking, elbow bending, and finger bending) and slight movement monitoring(including respiration recognition and swallowing recognition). As shown in Fig. 8b and c, the C-NGGK pressure sensor is attached on the finger and elbow to detect human joint actions (elbow and finger bendings). When the finger and elbow continuously bend, significantly relative variations of resistance in the sensor are collected. The C-NGGK pressure sensor is also applied to monitor walking speed. The C-NGGK sensor is attached on the knee joint to recognize the walking motions of a person (Fig. 8d). When a person walks in similar gait and stride at different speed, the sensor shows similar signal intensities but different signal frequencies. Besides, the C-NGGK pressure sensor exhibited an ultrahigh sensitivity to small forces. The sensor that attached on a person's chest have captured slight muscle movements during breathing (Fig. 8e). The flexible C-NGGK sensor attached on the neck can detect the relative variations of resistance caused by swallowing (Fig. 8f). These results suggest the promising applications of the carbon aerogel in pressure sensors and various wearable devices.

4. Conclusions

In conclusion, the well-designed hierarchical wave-shape architecture overcomes the brittleness of the carbonaceous materials. Carbonized CNF is beneficial to the enhancement of resistance to deformation and acts as a nano-enhancement or support; carbonized glucose exhibit the potential to form interactions between adjacent rGO layers; carbonized kaolin has excellent hydrophobicity, the addition of kaolin as a precursor of C-NGGK contributes to the formation of hydrophobic composite carbon aerogel. Those properties endow the C-NGGK with superhydrophobic, superelasticity, excellent fatigue resistance and stable strain-current response. Particularly, the absorption of C-NGGK resulted in 75–225 times of their own weights for organic contaminants and oils, demonstrating excellent reusability, durability and fire resistance. Benefiting from the unique structural feature and added composite components, C-NGGK can be an ideal candidate for environmental protection (industrial sewage treatments or oil spill cleanup) and pressure sensors. Moreover, the additional potentials of the C-NGGK would include 3D electrode materials for supercapacitors and batteries, catalyst carriers and various wearable devices.

Author contributions section

Sishi Long, The main writer and experimenter.
Yunchao Feng, Contributed to the experiment of compression,

elasticity and cycling tests.

Faliang He, Contributed to the experiment of C-NGGK sensor.

Shuaishuai He, Contributed to the experiment of CNF preparation.

Huachi Hong, Contributed to the experiment of fabrication of CNF-GO/glucose-kaolin suspension.

Xuerui Yang, Contributed to the experiment of electrochemistry.

Lingling Zheng, Contributed to the experiment of TEM and SEM.

Jian Liu, Professor and one of the viewpoint proposers.

Lihui Gan, Assistant professor and one of the viewpoint proposers.

Minnan Long, One of the professors of the lab, contributed to the experiment design.

Declaration of competing interest

There are no conflicts of interest to declare.

Acknowledgements

This work was supported by National Natural Science Foundation of China (No. 21978249) and Energy Development Foundation of Energy College, Xiamen University (No. 2018NYFZ03 & 2017NYFZ02).

Appendix A. Supplementary data

Supplementary data to this article can be found online at https://doi.org/10.1016/j.carbon.2019.11.065.

References

[1] Y. Si, X. Wang, C. Yan, L. Yang, J. Yu, B. Ding, Adv. Mater. 28 (2016), 9655-9655.
[2] H. Zhuo, Y. Hu, X. Tong, Z. Chen, L. Zhong, H. Lai, L. Liu, S. Jing, Q. Liu, C. Liu, Adv. Mater. 30 (2018) 1706705.
[3] B. Wang, D. Li, M. Tang, H. Ma, Y. Gui, X. Tian, F. Quan, X. Song, Y. Xia, J. Alloy. Comp. 749 (2018) 517–522.
[4] R.J. White, N. Yoshizawa, M. Antonietti, M.-M. Titirici, Green Chem. 13 (2011) 2428.
[5] D. Yuan, T. Zhang, Q. Guo, F. Qiu, D. Yang, Z. Ou, Chem. Eng. J. 351 (2018) 622–630.
[6] Z.-Y. Wu, C. Li, H.-W. Liang, Y.-N. Zhang, X. Wang, J.-F. Chen, S.-H. Yu, Sci. Rep. (2014) 4.
[7] X. Dong, J. Chen, Y. Ma, J. Wang, M.B. Chan-Park, X. Liu, L. Wang, W. Huang, P. Chen, Chem. Commun. 48 (2012) 10660–10662.
[8] X. Gui, J. Wei, K. Wang, A. Cao, H. Zhu, Y. Jia, Q. Shu, D. Wu, Adv. Mater. 22 (2010) 617–621.
[9] Z.-S. Wu, S. Yang, Y. Sun, K. Parvez, X. Feng, K. Müllen, J. Am. Chem. Soc. 134 (2012) 9082–9085.
[10] S. Zhou, G. Chen, X. Feng, M. Wang, T. Song, D. Liu, F. Lu, H. Qi, Green Chem. 20 (2018) 3593–3603.
[11] S.C. Li, B.C. Hu, Y.W. Ding, H.W. Liang, C. Li, Z.Y. Yu, Z.Y. Wu, W.S. Chen, S.H. Yu, Angew. Chem. 130 (2018).
[12] Y. Zhang, W. Fan, H. Lu, T. Liu, Electrochim. Acta 283 (2018) 1763–1772.
[13] L. E, W. Li, C. Ma, Z. Xu, S. Liu, Appl. Surf. Sci. 457 (2018) 477–486.
[14] D. Luo, S. Liu, F. Lin, L. Yu, J. Zhang, Solid State Ion. 321 (2018) 1–7.
[15] C. Zhang, S. Liu, Y. Qi, F. Cui, X. Yang, Chem. Eng. J. 351 (2018) 825–831.
[16] F. Yavari, Z. Chen, A.V. Thomas, W. Ren, H.M. Cheng, N. Koratkar, Sci. Rep. 1 (2011) 166.
[17] A. Ding, Int. J. Electrochem. Sci. (2018) 4379–4389.
[18] H. Sun, Z. Xu, C. Gao, Adv. Mater. 25 (2013) 2554–2560.
[19] Z.Y. Wu, C. Li, H.W. Liang, J.F. Chen, S.H. Yu, Angew. Chem. 52 (2013) 2925–2929.
[20] R.W. Pekala, C.T. Alviso, F.M. Kong, S.S. Hulsey, J. Non-Cryst. Solids 145 (1992) 90–98.
[21] D. Wu, R. Fu, S. Zhang, M.S. Dresselhaus, G. Dresselhaus, Carbon 42 (2004) 2033–2039.
[22] R. Fu, B. Zheng, J. Liu, M.S. Dresselhaus, G. Dresselhaus, J.H. Satcher Jr., T.F. Baumann, Adv. Funct. Mater. 13 (2003) 558–562.
[23] R. Zhang, Y. Cao, P. Li, X. Zang, P. Sun, K. Wang, M. Zhong, J. Wei, D. Wu, F. Kang, H. Zhu, Nano Res. 7 (2014) 1477–1487.
[24] S. Barg, F.M. Perez, N. Ni, P. do Vale Pereira, R.C. Maher, E. Garcia-Tuñon, S. Eslava, S. Agnoli, C. Mattevi, E. Saiz, Nat. Commun. 5 (2014).
[25] Z. Chen, W. Ren, L. Gao, B. Liu, S. Pei, H.-M. Cheng, Nat. Mater. 10 (2011) 424.
[26] H.-P. Cong, X.-C. Ren, P. Wang, S.-H. Yu, ACS Nano 6 (2012) 2693–2703.
[27] M. Kotal, H. Kim, S. Roy, I.-K. Oh, J. Mater. Chem. 5 (2017) 17253–17266.
[28] L. Qiu, J.Z. Liu, S.L. Chang, Y. Wu, D. Li, Nat. Commun. 3 (2012) 1241.
[29] H. Zhuo, Y. Hu, X. Tong, Z. Chen, L. Zhong, H. Lai, L. Liu, S. Jing, Q. Liu, C. Liu, X. Peng, R. Sun, Adv. Mater. 30 (2018), e1706705.
[30] J. Kuang, L. Liu, Y. Gao, D. Zhou, Z. Chen, B. Han, Z. Zhang, Nanoscale 5 (2013) 12171–12177.
[31] H. Bi, I.W. Chen, T. Lin, F. Huang, Adv. Mater. 27 (2015) 5943–5949.
[32] K.H. Kim, M.N. Tsui, M.F. Islam, Chem. Mater. 29 (2017) 2748–2755.
[33] H.L. Gao, Y.B. Zhu, L.B. Mao, F.C. Wang, X.S. Luo, Y.Y. Liu, Y. Lu, Z. Pan, J. Ge, W. Shen, Y.R. Zheng, L. Xu, L.J. Wang, W.H. Xu, H.A. Wu, S.H. Yu, Nat. Commun. 7 (2016) 12920.
[34] L. Estevez, A. Kelarakis, Q. Gong, E.H. Da'as, E.P. Giannelis, J. Am. Chem. Soc. 133 (2011) 6122–6125.
[35] J.L. Vickery, A.J. Patil, S. Mann, Adv. Mater. 21 (2009) 2180–2184.
[36] H.W. Liang, Q.F. Guan, L.F. Chen, Z. Zhu, W.J. Zhang, S.H. Yu, Angew. Chem. 51 (2012) 5101–5105.
[37] Y. Kuang, C. Chen, G. Pastel, Y. Li, J. Song, R. Mi, W. Kong, B. Liu, Y. Jiang, K. Yang, L. Hu, Adv. Energy Mater. 8 (2018) 1802398.
[38] M. Liu, P. Zhang, Z. Qu, Y. Yan, C. Lai, T. Liu, S. Zhang, Nat. Commun. 10 (2019) 3917.
[39] T. Saito, S. Kimura, Y. Nishiyama, A. Isogai, Biomacromolecules 8 (2007) 2485–2491.
[40] D. Klemm, F. Kramer, S. Moritz, T. Lindström, M. Ankerfors, D. Gray, A. Dorris, Angew. Chem. Int. Ed. 50 (2011) 5438–5466.
[41] S. Iwamoto, W. Kai, A. Isogai, T. Iwata, Biomacromolecules 10 (2009) 2571–2576.
[42] A. Jänes, H. Kurig, E. Lust, Carbon 45 (2007) 1226–1233.
[43] F. Bonhomme, J. Lassegues, L. Servant, J. Electrochem. Soc. 148 (2001) E450–E458.
[44] J. Suhr, P. Victor, L. Ci, S. Sreekala, X. Zhang, O. Nalamasu, P. Ajayan, Nat. Nanotechnol. 2 (2007) 417.
[45] L. Qiu, B. Huang, Z. He, Y. Wang, Z. Tian, J.Z. Liu, K. Wang, J. Song, T.R. Gengenbach, D. Li, Adv. Mater. 29 (2017) 1701553.
[46] Y.-J. Wan, P.-L. Zhu, S.-H. Yu, R. Sun, C.-P. Wong, W.-H. Liao, Carbon 115 (2017) 629–639.
[47] X. Wang, L.L. Lu, Z.L. Yu, X.W. Xu, Y.R. Zheng, S.H. Yu, Angew. Chem. Int. Ed. 54 (2015) 2397–2401.
[48] J. Song, C. Chen, Z. Yang, Y. Kuang, T. Li, Y. Li, H. Huang, I. Kierzewski, B. Liu, S. He, ACS Nano 12 (2017) 140–147.
[49] Y. Zhang, Z. Lu, Z. Yang, D. Zhang, J. Li, J. Shi, Z. Yuan, H. Chen, Carbon 155 (2019) 344–352.
[50] H. Sun, Z. Xu, C. Gao, Adv. Mater. 25 (2013) 2554–2560.
[51] H. Hu, Z. Zhao, W. Wan, Y. Gogotsi, J. Qiu, Adv. Mater. 25 (2013) 2219–2223.
[52] S. Barg, F.M. Perez, N. Ni, P. do Vale Pereira, R.C. Maher, E. Garcia-Tunon, S. Eslava, S. Agnoli, C. Mattevi, E. Saiz, Nat. Commun. 5 (2014) 4328.
[53] X. Gui, J. Wei, K. Wang, A. Cao, H. Zhu, Y. Jia, Q. Shu, D. Wu, Adv. Mater. 22 (2010) 617–621.
[54] T.A. Schaedler, A.J. Jacobsen, A. Torrents, A.E. Sorensen, J. Lian, J.R. Greer, L. Valdevit, W.B. Carter, Science 334 (2011) 962–965.
[55] Y. Si, J. Yu, X. Tang, J. Ge, B. Ding, Nat. Commun. 5 (2014) 5802.
[56] K. Xiao, L.X. Ding, G. Liu, H. Chen, S. Wang, H. Wang, Adv. Mater. 28 (2016) 5997–6002.
[57] H.W. Liang, Q.F. Guan, L.F. Chen, Z. Zhu, W.J. Zhang, S.H. Yu, Angew. Chem. Int. Ed. 51 (2012) 5101–5105.
[58] L. Qiu, J.Z. Liu, S.L. Chang, Y. Wu, D. Li, Nat. Commun. 3 (2012) 1241.
[59] A. Cao, P.L. Dickrell, W.G. Sawyer, M.N. Ghasemi-Nejhad, P.M. Ajayan, Science 310 (2005) 1307–1310.